LETTER

doi:10.1038/nature14354

In situ low-relief landscape formation as a result of river network disruption

Rong Yang[1], Sean D. Willett[1] & Liran Goren[2]

Landscapes on Earth retain a record of the tectonic, environmental and climatic history under which they formed. Landscapes tend towards an equilibrium in which rivers attain a stable grade that balances the tectonic production of elevation and with hillslopes that attain a gradient steep enough to transport material to river channels. Equilibrium low-relief surfaces are typically found at low elevations, graded to sea level. However, there are many examples of high-elevation, low-relief surfaces, often referred to as relict landscapes[1,2], or as elevated peneplains[3]. These do not grade to sea level and are typically interpreted as uplifted old landscapes, preserving former, more moderate tectonic conditions[4]. Here we test this model of landscape evolution through digital topographic analysis of a set of purportedly relict landscapes on the southeastern margin of the Tibetan Plateau, one of the most geographically complex, climatically varied and biologically diverse regions of the world. We find that, in contrast to theory, the purported surfaces are not consistent with progressive establishment of a new, steeper, river grade, and therefore they cannot necessarily be interpreted as a remnant of an old, low relief surface. We propose an alternative model, supported by numerical experiments, in which tectonic deformation has disrupted the regional river network, leaving remnants of it isolated and starved of drainage area and thus unable to balance tectonic uplift. The implication is that the state of low relief with low erosion rate is developing *in situ*, rather than preserving past erosional conditions.

The Tibetan Plateau has uplifted over the past approximately 50 million years (Myr) and has been argued to be growing eastwards through a combination of block motion on strike-slip faults[5–7], uplift in response to lower crustal flow[8] and large-scale shortening in response to indentation of the Indian plate[9]. To the southeast of the plateau proper is a topographic transition, referred to as the 'Three Rivers' region, taking its name from the three large rivers (Salween, Mekong and Yangtze) that have incised the edge of the plateau, forming bedrock gorges up to 3 km deep (Fig. 1). Although surface expression of tectonic activity is not always evident, large strike-slip faults parallel the main rivers[10] and there is evidence for tectonic disturbance to the landscape, including captures of major rivers[11,12]. Geodynamic models suggest that the region, situated near the corner of the indenting India plate, has been subjected to large horizontal strains[9,13]. Thermochronometry suggests that the major rivers accelerated their incision about 10 Myr ago (Ma), although paleo-altimetry based on stable isotope data suggests that most of the area has been near its current elevation for more than 40 Myr[14,15]. A regional low-relief surface, or relict landscape, with low erosion rates[16–19] has been identified in the headwaters of the three rivers and along the interfluves in the middle and lower reaches, and its existence has been used to argue for relatively recent uplift[1,20].

The transient response of a landscape to a change in uplift rate is dominated by changes in river channel slope. Channel slope has a first-order dependence on discharge or its proxy, drainage area, so measures of channel slope must be normalized for drainage area. Similar to past treatments of the problem[21–23], we transform distance from base level, x, along the channel to the surrogate quantity, χ:

$$\chi(x) = \int_0^x \left(\frac{P_0 A_0}{A(x')P(x')} \right)^{\frac{m}{n}} \mathrm{d}x' \quad (1)$$

where m and n are empirical, non-integer constants, P is precipitation rate and A is the upstream drainage area[24]. P_0 and A_0 are arbitrary scaling factors for the precipitation rate and drainage area, respectively. The change in channel elevation with respect to χ is referred to as channel steepness and provides a measure of the local erosion rate. For

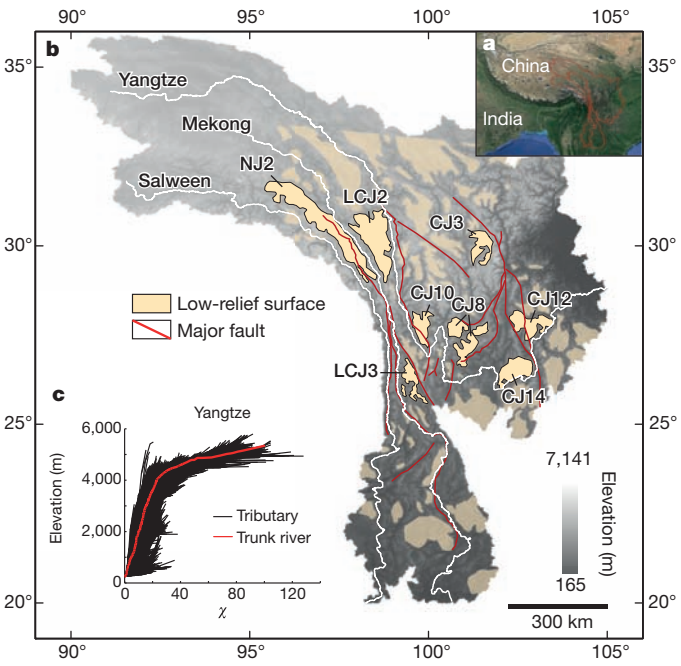

Figure 1 | The study area of the 'Three Rivers'. **a**, The catchment boundaries of the Salween, Mekong and Yangtze Rivers in southeast Asia. **b**, Map of low-relief areas within the 'Three Rivers' region. Trunk channel of the Salween, Mekong and Yangtze Rivers shown in white. Major faults shown in red. Yellow shading indicates low-relief surfaces as identified in ref. 1. Surfaces singled out for our study and shown in subsequent figures are labelled. **c**, Normalized elevation plot (χ-plot) for the Yangtze. Red curve is the profile of the main stem. χ is calculated from equation (1) using $m/n = 0.45$. Precipitation rate is shown in Extended Data Fig. 1. The comparable information for the Salween and Mekong is shown in Extended Data Fig. 2. The same data for a range of values of m/n are shown in Extended Data Fig. 2. Erosion rate scales with the slope of the plot[22], so the scatter in the slope of the tributaries implies variability in the erosion rate[17].

[1]Geological Institute, Swiss Federal Institute of Technology, 8092 Zurich, Switzerland. [2]Geological and Environmental Sciences, Ben-Gurion University of the Negev, Beer-Sheva 84105, Israel.

a steady, constant uplift rate, erosion rate equals the uplift rate and the channel steepness, K_s, is proportional to the uplift rate, U, as

$$K_s = \left(\frac{U}{KA_0^m}\right)^{\frac{1}{n}} \quad (2)$$

where K reflects the basin runoff characteristics and rock erodibility[25]. According to prevailing theory, a channel steepness transient initiates at base level and propagates upstream as a kinematic wave[25–27]. By normalizing for drainage area, we can compare rivers of variable size across a landscape given that channels with a common uplift pattern and history should collapse onto a single profile in elevation–χ space[22]. Even with added complexities in the incision law[28], area–slope scaling at steady state remains a robust feature of most landscapes, so that a χ-plot gives a valuable metric for the state of disequilibrium. The χ-plot of the Yangtze River above the Sichuan Basin using the precipitation data from the Tropical Rainfall Measurement Mission (Extended Data Fig. 1) shows high steepness for χ less than about 20 and much lower steepness for larger χ (Fig. 1c), reflecting the low relief of the Tibetan plateau. However, scatter in this plot is very large at all elevations. The Salween and Mekong Rivers exhibit similarly large scatter (Extended Data Fig. 2). This variability in steepness is consistent with the existence of low-steepness landscape fragments throughout the region, but it is not consistent with the idea of a common history of uplift. However, over a region as large as the 'Three Rivers', we expect temporal and spatial variations in uplift and rock erodibility, so the analysis is best applied at a smaller scale.

To test whether there is a common uplift history for individual low-relief surfaces, we generated χ-plots for the rivers draining the interior of individual 'relict' surfaces as identified in ref. 1. These profiles were compared with profiles of the rivers draining the exterior of the low-relief landscape and with the main trunk of the nearest of the three rivers. We attempted to select low-relief landscapes interior to one of the three major drainage basins, and only considered tributary rivers having a common confluence close to the low-relief surface. Any differences between channel profiles must arise above their common confluence, confirming that we were looking at local processes. In total, we investigated eight regions (Fig. 2 and Extended Data Figs 3–9).

All regions showed remarkably consistent river profile characteristics (see, for example, Fig. 2). It is clear that there is no common uplift history that can explain the aggregate set of rivers, even in the limited area of a single low-relief surface, and independent of the selection of exponents in equation (1) (Extended Data Fig. 2). The kinematic wave model of channel equilibration predicts collapse of all rivers onto a single elevation–χ profile[22], which is not observed. All tributaries mapped in Fig. 2 deviate in steepness, as represented by the slope of the χ-plot, upstream from their confluence with the main stem of the Yangtze River. What is most remarkable is that they deviate systematically. All rivers draining the interior of the low-relief surface plot below the regional average; all rivers draining the exterior perimeter of the surface have a steeper slope and plot above the interior-draining rivers and above the trunk river. In every case, there is a specific range of χ over which the interior river channels have a lower steepness than the exterior channels. In addition, the large contrast in χ across water divides surrounding the low-relief catchments suggests that the regional network does not have a stable geometry and thus does not retain an old, near-equilibrium state[21]. Differences in steepness can arise from differences in rock erodibility, uplift rate or precipitation rate, and individual features may be attributed to these factors; however, given the restricted area of each of these examples, and the individual geometry of each low-relief surface, we can exclude these factors as a general explanation for the pattern of river profile diversity in all eight areas.

The other potential source of variation in the χ-plots arises from changes in drainage basin area by river capture and divide migration.

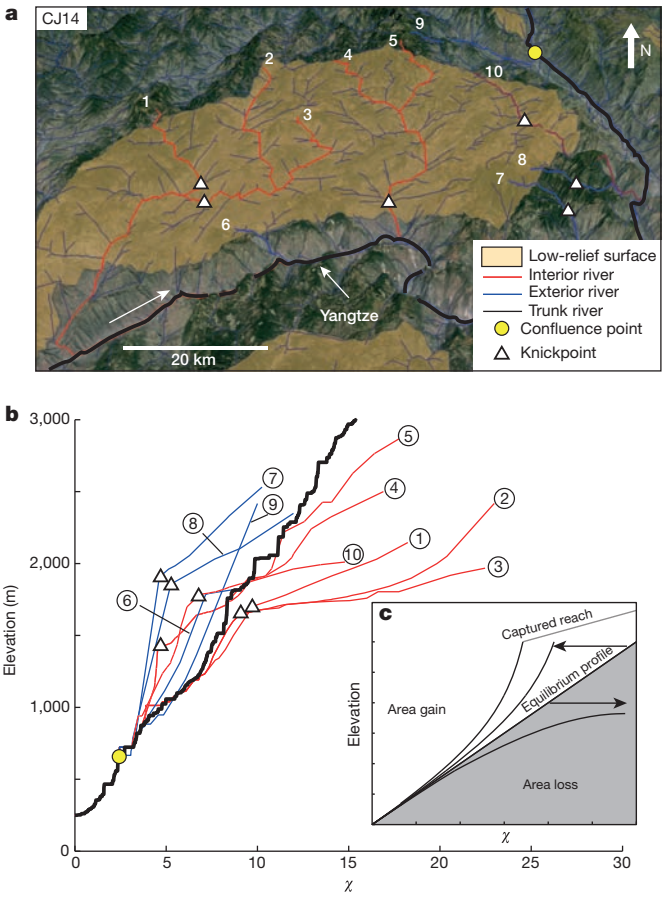

Figure 2 | River courses and χ-plots for region of low-relief, 'relict' landscape CJ14 in the Yangtze drainage. See Fig. 1 for location. **a**, Perspective view of the landscape. The low-relief surface is shaded and the courses of ten rivers are keyed by colour and number to the χ-plots in **b**. **b**, Graph of χ-plots for rivers shown in Fig. 2a. Red tributaries are primarily interior to the low-relief landscape; blue rivers drain the exterior. Yellow point in each frame shows downstream point common to all rivers. Triangles indicate prominent inflections in profiles and their locations in Fig. 2a. **c**, Schematic of response of χ-plot to instantaneous area change or discrete river capture. Loss of drainage area shifts plot to the right; gain of area shifts plot to the left. A discrete capture event may preserve the slope of the captured reach. Note that interior rivers (1, 2, 3) are all shifted into the area-loss field, although the lower reaches may have equilibrated with the main stem of the Yangtze. Tributaries 4–10 are shifted into the area-gain field. Tributaries 4, 5, 7, 8 and 10 appear to have recently captured additional area from the upper surface, thus exhibiting a kinked profile. Examples of this analysis applied to other low-relief landscapes are shown in Extended Data Figs 3–9.

Temporal changes in drainage area produce distinctive changes in the χ-profiles[21]. Given that χ depends inversely on drainage area, a loss of area pushes an equilibrium profile towards higher χ, preferentially affecting the upper reaches of a river, as shown in Fig. 2c. Conversely, an increase in drainage area decreases χ, pulling the profile to the left in a χ-plot. In the case of a large river capture, the river below the capture point is pulled to the left and its plot steepened, with the captured reach retaining its original slope, thus giving a distinctive, kinked plot (Fig. 2c). In all cases, area change leads to a disequilibrium state of the river channel, which will evolve back towards equilibrium through changes in erosion rate and channel steepness. There is an important positive feedback to this process, in that, during the disequilibrium phase, area loss leads to a lower erosion rate and thereby to surface uplift and higher elevation. Higher elevation increases vulnerability to further area loss by either capture or divide migration. A river that is the victim of drainage-area loss is therefore characterized by high

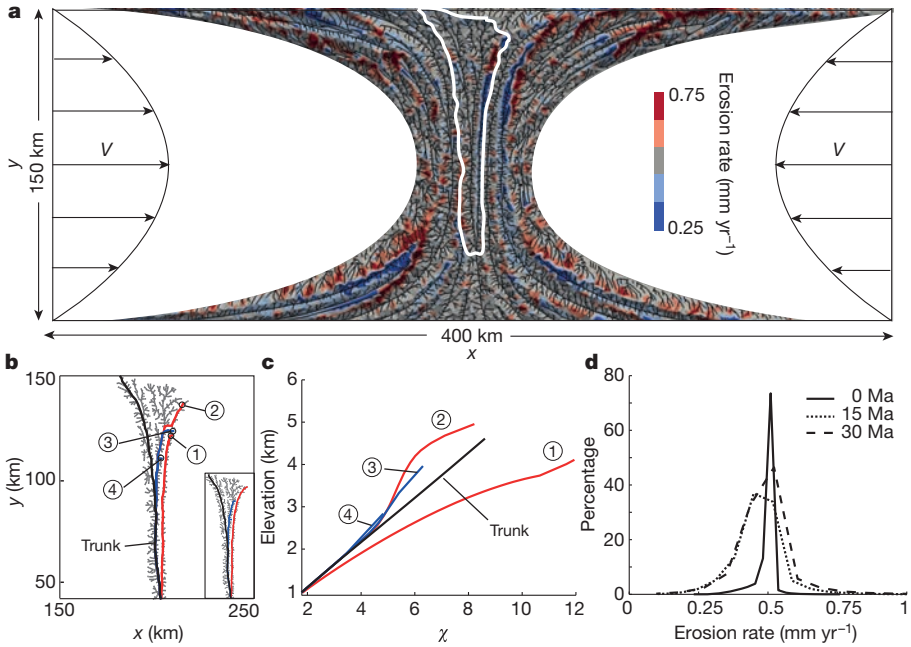

Figure 3 | Numerical model of landscape evolution governed by stream-power river incision in response to tectonic uplift and horizontal strain using the Divide and Capture (DAC) landscape evolution model[29]. **a**, River network configuration and erosion rate shown at model time of 25.8 Myr. Tectonic rock uplift rate is constant in space and time at 0.5 mm yr^{-1}. Initial topography is near steady state with the same uplift rate and no horizontal motion. All boundaries are fixed elevation at nominal sea level. At time zero, domain is subjected to horizontal contractive field with a double parabolic form and a maximum velocity of 15 mm yr^{-1} (see Methods). Shortening vectors shown as black arrows. Only lower (south) half of the symmetrical model is shown, so upper (north) edge of figure is approximately the main divide of an approximately symmetric domain. Full model is shown in the Supplementary Video. **b**, A select drainage basin (see location highlighted in white in **a**) exhibiting typical erosion rate variations. The red segment of river 2 has been captured from river 1. The inset shows the drainage basin configuration just before river capture. **c**, Graph of χ-plot of river basin shown in **b**. River steepness (slope of χ-plot) is low in tributaries that have recently lost area and high in tributaries that have gained area. Note similarities in overall basin structure with natural example in Fig. 2. **d**, Distribution of erosion rate across full model domain at three times, showing increase in erosion rate variance in response to tectonic strain. Note decrease in mean and negative skewness in distribution, reflecting the perseverance of low-erosion rate regions.

elevation, low channel steepness, low erosion rates and is typically surrounded by rivers that are aggressively advancing into its current drainage basin[21]. These are precisely the characteristics of the regional landscapes portrayed here (Fig. 2 and Extended Data Figs 3–9).

To demonstrate this mechanism and to show that tectonic shortening and shear deformation does produce such a landscape, we constructed a numerical model of a landscape experiencing a non-uniform shortening rate representing the indentation of the Indian plate into southeast Asia[9,13]. The model solves for stream-power incision of river channels in a river network, subjected to tectonic uplift and horizontal motion, and includes an explicit description of the water divide motion[29] (Methods). In our numerical experiment (Fig. 3 and Supplementary Video), we impose a pincer-type horizontal strain-rate field on an initially steady state topography, but retain the initial rock uplift rate. The tectonic strain deforms the river basins and induces multiple river captures as the channel network attempts to regain a more stable configuration. These changes in network configuration also induce variations in river steepness (Fig. 2c) with a corresponding increase in variance of erosion rate (equation (2)). In particular, a large fraction of the model domain has erosion rates lower or higher than the imposed tectonic uplift rate (Fig. 3d). Low erosion rates are in part due to the lengthening of flow paths by extensional strain, but the lowest erosion rate regions are typically victims of a large river capture. Given the area-loss feedback, these low-erosion-rate regions are subject to multiple subsequent captures, as well as continuous inward divide migration by steeper neighbouring basins. These processes prolong the transient phase of landscape response and result in isolated catchments with anomalously high elevations and low erosion rates, much as is observed in the 'Three Rivers' region (compare Fig. 3c with Fig. 2b or Extended Data Figs 3–9).

Our numerical model includes several simplifications. The imposed strain field is continuous, whereas in nature surface deformation is commonly brittle, with localized faults. The use of a continuous strain field has the tendency to minimize channel network disruption; the same strain distributed across discrete faults would probably have a much larger effect on the channel network geometry. We also do not include sediment production and deposition in our model. A river that loses upstream area loses sediment carrying capacity and may not be able to transport sediment supplied by local hillslopes. This sediment would be locally deposited, preventing additional channel erosion[28]. Thus our model provides a minimum estimate of the variations in erosion rate expected through channel network disruption.

Drainage basin disruption slows, but does not prevent the re-equilibration of low erosion rate catchments to base level; in fact, we observe steepening of the lower reaches of many rivers with convex inflections separating steep and gentle river segments (Fig. 2 and Extended Data Figs 3–9). However, the height and position of these inflections are typically unique to an individual drainage basin, inconsistent with the idea of a regional wave of incision propagating upstream. As an end-member interpretation, each low-relief catchment could correspond to a specific large capture event. In some cases, it is possible to determine this. For example, surface CJ12 (Extended Data Fig. 8) is downstream from the former course of the Dadu River[12]. However, in most cases, low-relief surfaces result not from a single event, but through a series of captures accompanied by continuous divide migration, making it difficult to assign attribution to a single event. We also cannot exclude the possibility that much of the region has experienced an acceleration in rock uplift. In fact, an increase in uplift rate would be expected to accompany the shortening of our simulation. In addition, the upper 'Three Rivers' region drains

the Tibetan Plateau, whose existence over a much larger area suggests that other tectonic or climatic processes are important to formation of the plateau landscape that includes the uppermost low-relief surfaces[30]. However, our model suggests that an acceleration in uplift rate is not required to form most of the landscape of the 'Three Rivers' region, nor is an initially low-relief landscape required. We suggest, rather, that the 'relict' landscapes are forming and being modified, *in situ* through loss of drainage area. Given the positive feedback inherent to drainage area loss and gain, it is unlikely that these, or any high, isolated surface will retain an unaltered record of past geomorphic conditions or elevations.

Online Content Methods, along with any additional Extended Data display items and Source Data, are available in the online version of the paper; references unique to these sections appear only in the online paper.

Received 16 June 2014; accepted 26 February 2015.

1. Clark, M. K. *et al.* Use of a regional, relict landscape to measure vertical deformation of the eastern Tibetan Plateau. *J. Geophys. Res.* **111,** http://dx.doi.org/10.1029/2005JF000294 (2006).
2. Schoenbohm, L. M., Whipple, K. X., Burchfiel, B. C. & Chen, L. Geomorphic constraints on surface uplift, exhumation, and plateau growth in the Red River region, Yunnan Province, China. *Geol. Soc. Am. Bull.* **116,** 895–909 (2004).
3. Davis, W. Baselevel, grade and peneplain. *J. Geol.* **10,** 77–111 (1902).
4. Babault, J., Van Den Driessche, J., Bonnet, S., Castelltort, S. & Crave, A. Origin of the highly elevated Pyrenean peneplain. *Tectonics* **24,** TC2010 (2005).
5. Tapponnier, P., Peltzer, G., Le Dain, A., Armijo, R. & Cobbold, P. Propagating extrusion tectonics in Asia: new insights from simple experiments with plasticine. *Geology* **10,** 611–616 (1982).
6. England, P. & Molnar, P. Right-lateral shear and rotation as the explanation for strike-slip faulting in eastern Tibet. *Nature* **344,** 140–142 (1990).
7. Tapponnier, P. Oblique stepwise rise and growth of the Tibet Plateau. *Science* **294,** 1671–1677 (2001).
8. Clark, M. K. & Royden, L. H. Topographic ooze: building the eastern margin of Tibet by lower crustal flow. *Geology* **28,** 703–706 (2000).
9. Hallet, B. & Molnar, P. Distorted drainage basins as markers of crustal strain east of the Himalaya. *J. Geophys. Res. Solid Earth* **106,** 13697–13709 (2001).
10. Burchfiel, B. C. & Chen, Z. *Tectonics of the Southeastern Tibetan Plateau and its Adjacent Foreland* 77–164 (Geological Society of America, 2012).
11. Clift, P. D., Blusztajn, J. & Nguyen, A. D. Large-scale drainage capture and surface uplift in eastern Tibet–SW China before 24 Ma inferred from sediments of the Hanoi Basin, Vietnam. *Geophys. Res. Lett.* **33,** http://dx.doi.org/10.1029/2006GL027772 (2006).
12. Clark, M. K. *et al.* Surface uplift, tectonics, and erosion of eastern Tibet from large-scale drainage patterns. *Tectonics* **23,** http://dx.doi.org/10.1029/2002TC001402 (2004).
13. England, P. & Houseman, G. Finite strain calculations of continental deformation. 2. Comparison with the India-Asia Collision Zone. *J. Geophys. Res.* **91,** 3664–3676 (1986).
14. Rowley, D. B. & Currie, B. S. Palaeo-altimetry of the late Eocene to Miocene Lunpola basin, central Tibet. *Nature* **439,** 677–681 (2006).
15. Hoke, G. D., Liu-Zeng, J., Hren, M. T., Wissink, G. K. & Garzione, C. N. Stable isotopes reveal high southeast Tibetan Plateau margin since the Paleogene. *Earth Planet. Sci. Lett.* **394,** 270–278 (2014).
16. Henck, A. C., Huntington, K. W., Stone, J. O., Montgomery, D. R. & Hallet, B. Spatial controls on erosion in the Three Rivers region, southeastern Tibet and southwestern China. *Earth Planet. Sci. Lett.* **303,** 71–83 (2011).
17. Ouimet, W. B., Whipple, K. X. & Granger, D. E. Beyond threshold hillslopes: Channel adjustment to base-level fall in tectonically active mountain ranges. *Geology* **37,** 579–582 (2009).
18. Duvall, A. R., Clark, M. K., Avdeev, B., Farley, K. A. & Chen, Z. Widespread late Cenozoic increase in erosion rates across the interior of eastern Tibet constrained by detrital low-temperature thermochronometry. *Tectonics* **31,** TC3014 (2012).
19. Wilson, C. J. L. & Fowler, A. P. Denudational response to surface uplift in east Tibet: evidence from apatite fission-track thermochronology. *Geol. Soc. Am. Bull.* **123,** 1966–1987 (2011).
20. Clark, M. K. *et al.* Late Cenozoic uplift of southeastern Tibet. *Geology* **33,** 525–528 (2005).
21. Willett, S. D., McCoy, S. W., Perron, J. T., Goren, L. & Chen, C. Y. Dynamic reorganization of river basins. *Science* **343,** http://dx.doi.org/10.1126/science.1248765.
22. Perron, J. T. & Royden, L. An integral approach to bedrock river profile analysis. *Earth Surf. Process. Landf.* **38,** 570–576 (2012).
23. Royden, L. & Taylor Perron, J. Solutions of the stream power equation and application to the evolution of river longitudinal profiles. *J. Geophys. Res. Earth Surf.* **118,** 497–518 (2013).
24. Ferrier, K. L., Huppert, K. L. & Perron, J. T. Climatic control of bedrock river incision. *Nature* **496,** 206–209 (2013).
25. Whipple, K. X. & Tucker, G. E. Dynamics of the stream-power river incision model: Implications for height limits of mountain ranges, landscape response timescales, and research needs. *J. Geophys. Res. Solid Earth* **104,** 17661–17674 (1999).
26. Seidl, M. & Dietrich, W. The problem of channel erosion into bedrock. *Catena, Suppl.* **23,** 101–124 (1992).
27. Weissel, J. & Seidl, M. in *Rivers over Rock: Fluvial Processes in Bedrock Channels* (American Geophysical Union Geophysical Monograph Series Vol. 107) (eds Tinkler, K. J. & Wohl, E. E.) 189–206 (American Geophysical Union, 1998).
28. Sklar, L. & Dietrich, W. E. in *Rivers over Rock: Fluvial Processes in Bedrock Channels* (American Geophysical Union Geophysical Monograph Series Vol. 107) (eds Tinkler, K. J. & Wohl, E. E.) 237–260 (American Geophysical Union, 1998).
29. Goren, L., Willett, S. D., Herman, F. & Braun, J. Coupled numerical-analytical approach to landscape evolution modeling. *Earth Surf. Process. Landf.* **39,** 522–545 (2014).
30. Liu-Zeng, J., Tapponnier, P., Gaudemer, Y. & Ding, L. Quantifying landscape differences across the Tibetan plateau: implications for topographic relief evolution. *J. Geophys. Res.* **113,** http://dx.doi.org/10.1029/2007JF000897 (2008).

Supplementary Information is available in the online version of the paper.

Acknowledgements We thank C.-Y. Chen for discussion and assistance with digital elevation model analysis. Reviews by D. Burbank improved the manuscript.

Author Contributions S.D.W. conceived and directed the project. R.Y. analysed the topography and precipitation. R.Y. and L.G. constructed the numerical model. All authors contributed to interpretation and writing.

Author Information Reprints and permissions information is available at www.nature.com/reprints. The authors declare no competing financial interests. Readers are welcome to comment on the online version of the paper. Correspondence and requests for materials should be addressed to R.Y. (rong.yang@erdw.ethz.ch).

METHODS

Topographic analysis was done using the SRTM3 digital elevation model, which has a resolution of approximately 90 m (ref. 31). A threshold drainage area of 5 km^2 was used to exclude regions dominated by debris flows or hillslope processes. We extracted all information such as longitude, latitude, elevation, flow direction, flow length, stream order and flow accumulation from the filled digital elevation model. The averaged annual precipitation rates were obtained with a spatial resolution of approximately 5 km × 5 km based on the 12-year Tropical Rainfall Measurement Mission data during the period 1998–2009 following the methods described in ref. 32. The χ-value for each pixel was calculated according to equation (1), using the Tropical Rainfall Measurement Mission precipitation data. Note that the equation (2) definition of χ corresponds to a version of χ' in ref. 21. Calculations were done assuming concavity $m/n = 0.45$, a scaling area A_0 of 1 m^2 and a scaling precipitation rate P_0 of 1 m yr^{-1}. This was selected according to the methodology in ref. 21. Other values of m/n are shown in Extended Data Fig. 2. Use of another concavity changes the position of the trunk river relative to the tributaries, but does not change the relative position or steepness of the interior- and exterior-draining rivers. To reduce the number of pixels for calculation, we applied a skipping factor; the data were resampled every five pixels for the Salween and Mekong and every ten pixels for the Yangtze but not for those pixels at confluences to maintain the river network structure. For the trunk river profile in Figs 2 and Extended Data Figs 3–9, flats due to filling were removed.

The landscape evolution simulation was generated using the coupled numerical–analytical model DAC (Divide and Capture)[29]. This model implements the physics of water divide motion and stream capture. We defined a rectangular domain size of 400 km × 300 km. We used $n = 1$ for the slope exponent, $m = 0.5$ for the area exponent and $K = 1.0 \times 10^{-6}$ for the rock erodibility. The simulation was initialized by generating a steady-state topography from an initially random (Gaussian, uncorrelated, maximum elevation of 1 m) elevation field with a spatially uniform tectonic uplift rate of 0.5 mm yr^{-1} and no horizontal motion. The base level on all four edges was fixed at a constant elevation, and precipitation rate and rock type were assumed to be steady and uniform. A symmetrical mountain range with maximum elevation of 5.4 km was generated after 100 Ma. Using this steady-state topography as an initial condition, we imposed a horizontal velocity field to simulate the shortening in response to indentation of the corner of the Indian plate into Eurasia. Horizontal velocity has non-zero component only in the x direction (east–west) and varies parabolically in the y direction (north–south) from the boundary to the centre line of the model. Velocity varies linearly in x, from maximum values at the boundaries to zero along the centre axis. The midpoint axes in both dimensions are thus symmetry conditions for the velocity field. Upper and lower halves of the model can be regarded as independent realizations of the indentation problem. The simulation starts at 0 Ma and ends at 30 Ma with a time step length of 500 years.

Code availability: the landscape evolution model and parameters are available from any of the authors on request.

31. Jarvis, A., Reuter, H. I., Nelson, A. & Guevara, E. Hole-filled SRTM for the globe v. 4 (http://srtmcsi.cgiar.org) (2008).
32. Bookhagen, B. & Strecker, M. R. Orographic barriers, high-resolution TRMM rainfall, and relief variations along the eastern Andes. *Geophys. Res. Lett.* **35,** http://dx.doi.org/10.1029/2007GL032011 (2008).
33. Xu, G. & Kamp, P. J. Tectonics and denudation adjacent to the Xianshuihe Fault, eastern Tibetan Plateau: constraints from fission track thermochronology. *J. Geophys. Res. Solid Earth* **105,** 19231–19251 (2000).

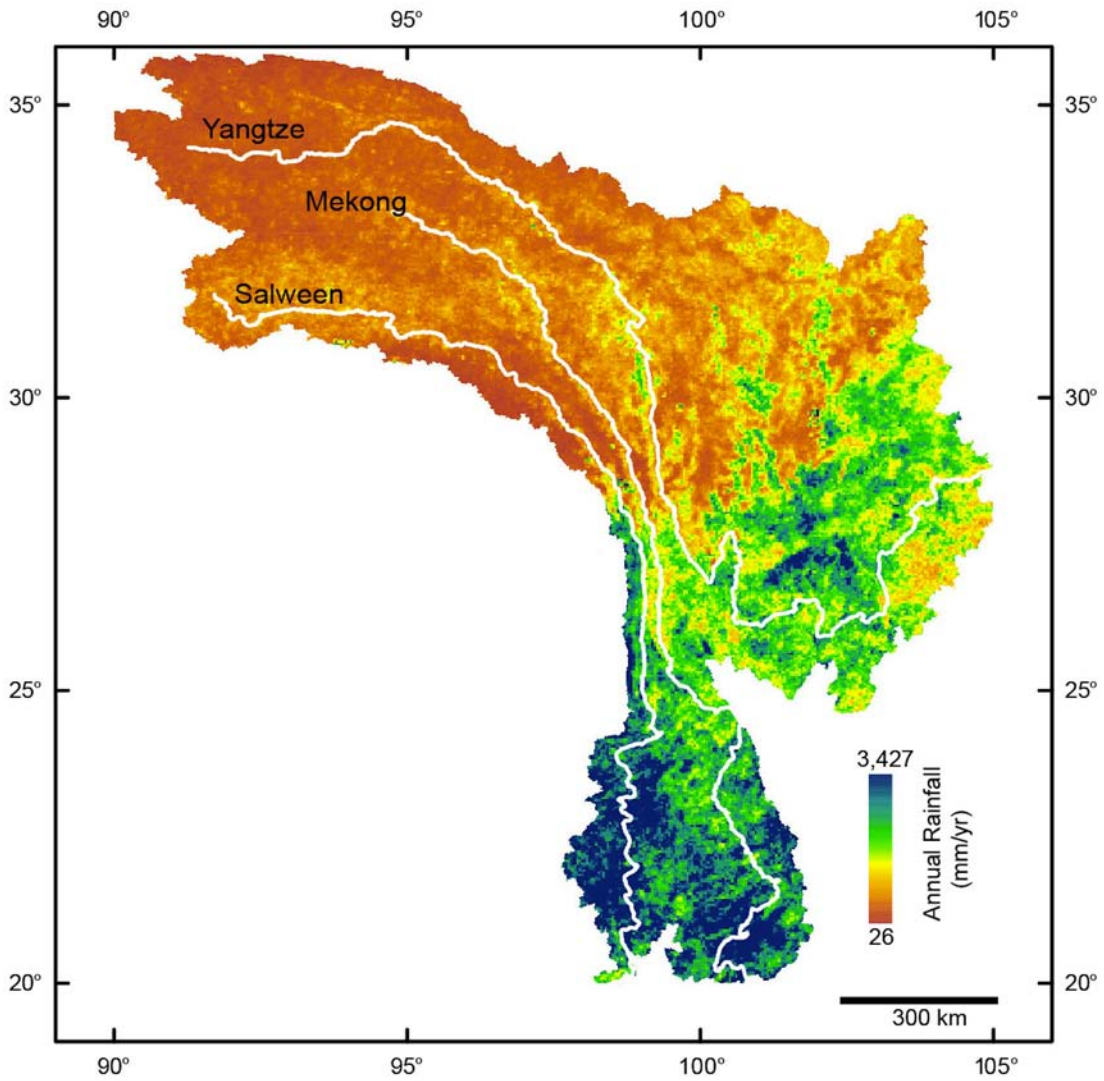

Extended Data Figure 1 | Mean annual precipitation for study area derived from Tropical Rainfall Measurement Mission data. See Methods.

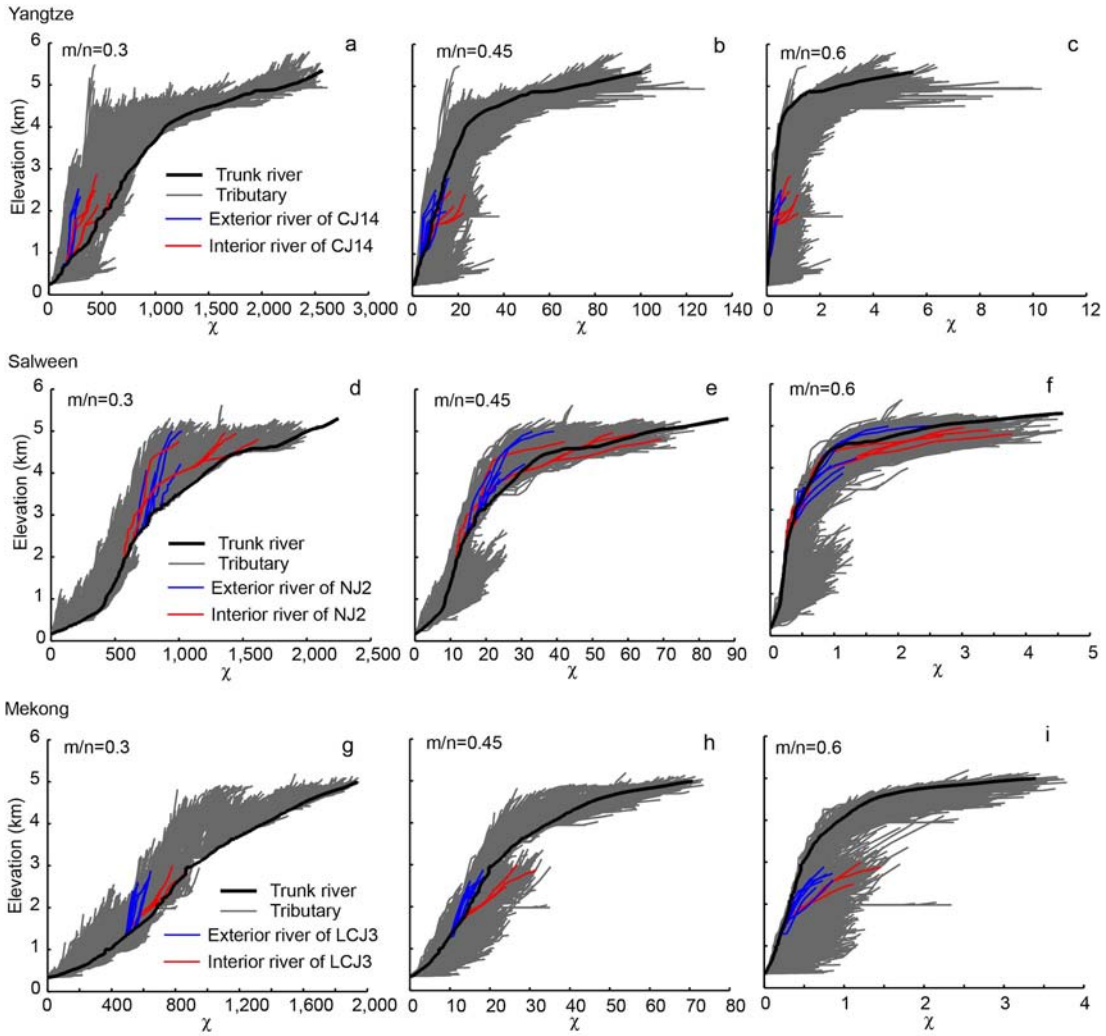

Extended Data Figure 2 | Yangtze, Salween and Mekong River χ-plots. Plots are constructed using a range of m/n from 0.3 to 0.6 to test the variability of χ-profiles with concavity. The trunk rivers are highlighted in black. We use a value of 0.45 for the χ analysis, following the methodology described in ref. 21.

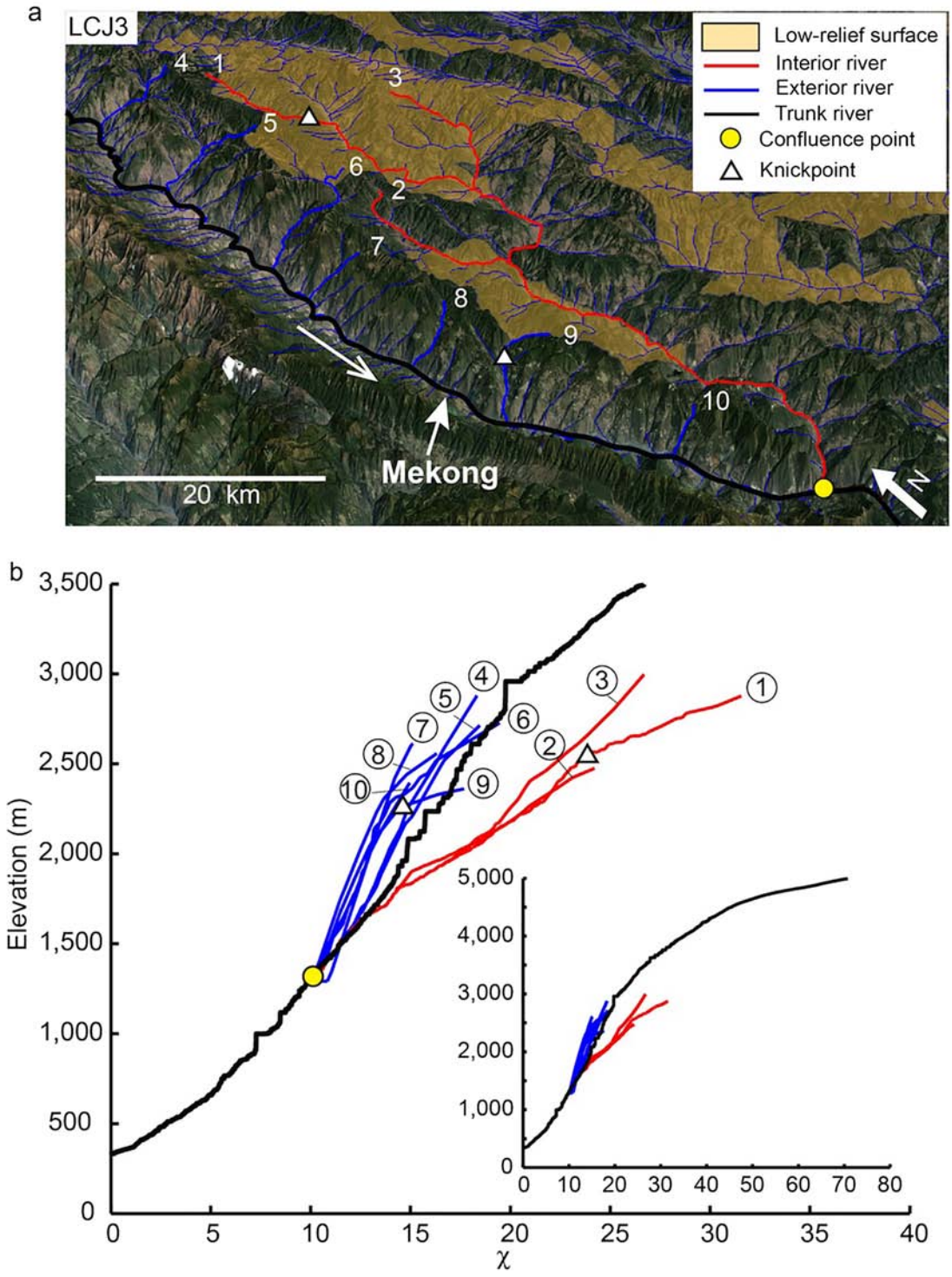

Extended Data Figure 3 | River courses and χ-plots for the region of low-relief landscape LCJ3 in the Mekong drainage. See Fig. 1 for location. **a**, Perspective view of the landscape. The low-relief surface is shaded and the courses of ten rivers are keyed by colour and number to the χ-plots in **b**. **b**, Graph of χ-plots for rivers shown in **a**. Inset shows same data, scaled to include the full Mekong. Red tributaries are primarily interior to the low-relief landscape; blue rivers drain the exterior. Bold black river is the trunk river with flow direction indicated by the white arrow. The yellow point in each frame shows the downstream point common to all rivers. Triangles indicate prominent inflections in profiles and their locations in **a**. Interior rivers (1, 2, 3) are all shifted towards lower erosion rates. Exterior rivers are all shifted towards higher erosion rates. Tributary 9 appears to include a recent headwater capture. The absence of common form to the χ-plots indicates no common uplift history. The independence of individual catchments suggests variance is due to changing catchment area.

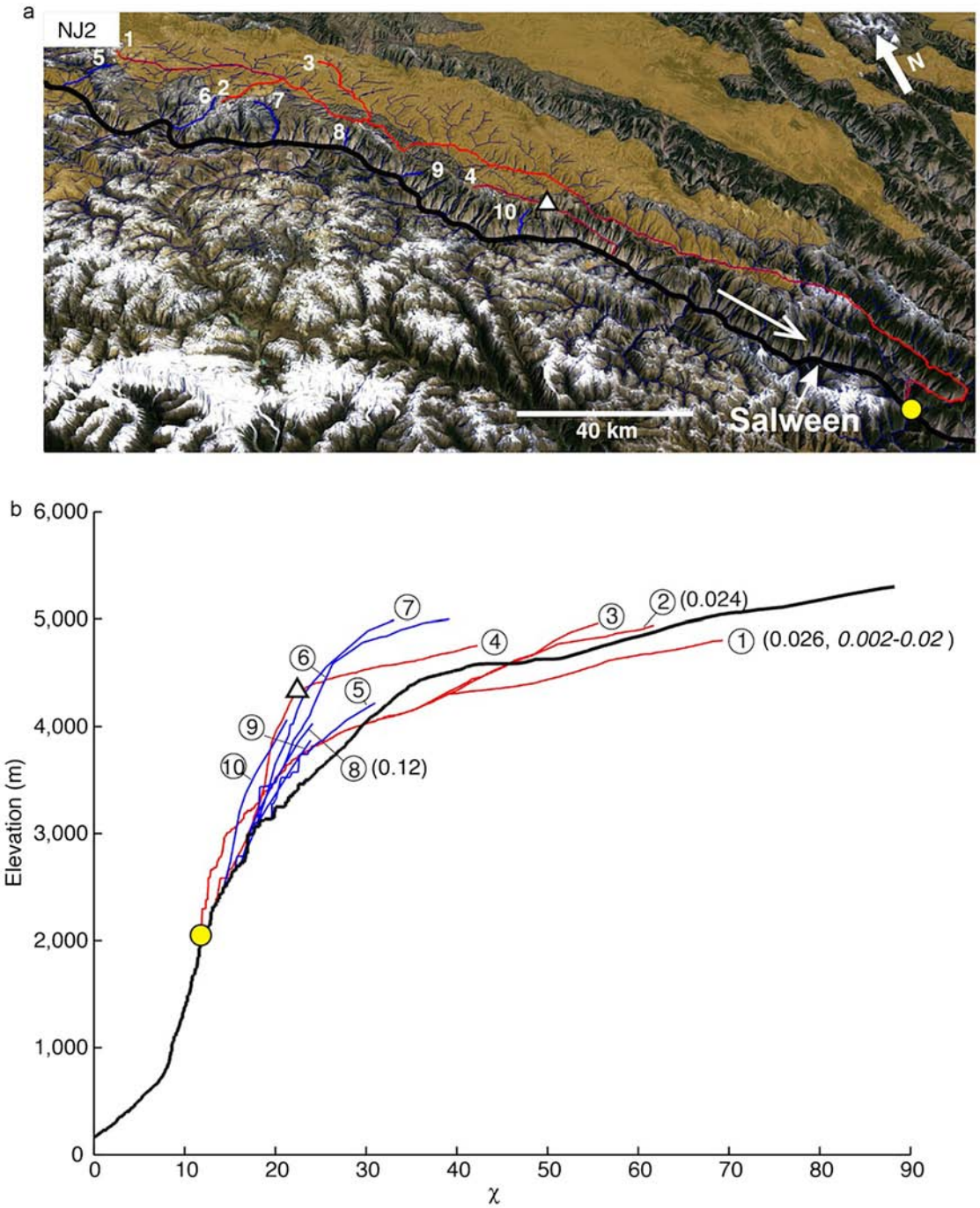

Extended Data Figure 4 | River courses and χ-plots for the region of low-relief landscape NJ2 in the Salween drainage. See Fig. 1 for location. Figure format as in Extended Data Fig. 3. **a**, Perspective view of the landscape. The low-relief surface is shaded and the courses of ten rivers are keyed by colour and number to the χ-plots in **b**. **b**, Graph of χ-plots for rivers shown in **a**. This surface is arguably part of the Tibetan Plateau proper and χ-values are nearly as large as the trunk river. Interior rivers (1, 2, 3) are all shifted into the area-loss field, although they are arguably not significantly different from the main stem. Tributary 4 includes a recent capture. Tributaries 5–10 are shifted into the area-gain field. Tributaries 6 and 7 might include captured reaches. Numbers in parentheses are erosion rates derived from ^{10}Be concentrations[16] or from thermochronometry (in italics)[18] and indicate a fivefold increase in erosion rate in exterior basin 8, relative to interior basins.

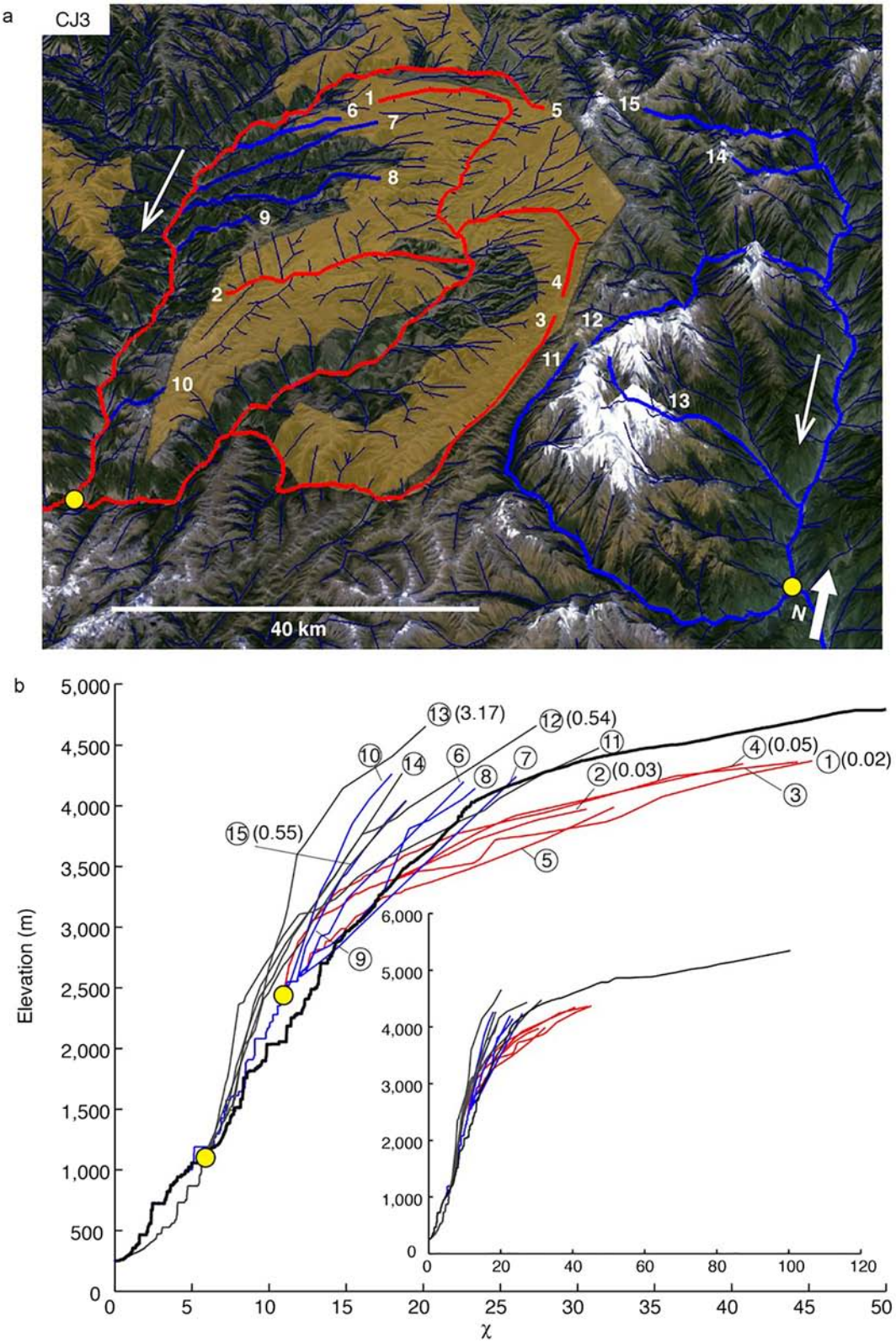

Extended Data Figure 5 | River courses and χ-plots for the region of low-relief landscape CJ3 in the Yangtze drainage. See Fig. 1 for location. Figure format as in Extended Data Fig. 3. **a**, Perspective view of the landscape. The low-relief surface is shaded and the courses of 15 rivers are keyed by colour and number to the χ-plots in **b**. **b**, Graph of χ-plots for rivers shown in **a**. Rivers 1–5 are shifted into the area-loss field, and may have been captured given their steep, common lower reach. Remaining rivers are either in equilibrium or are shifted into the area-gain field, although all rivers in this area have a lower reach steeper than the trunk of the Yangtze. Unique to this low-relief surface, we analysed tributaries with two, independent, common confluence points. Tributaries 11–15 have a common confluence independent of tributaries 1–10, so there is potential for different base level control on each set. In addition, this area is subject to anomalous uplift associated with the Gonga Shan massif[53]. These tributaries have been illustrated in grey in **b**. Numbers in parentheses are erosion rates derived from ^{10}Be concentrations[17] and indicate rates in the exterior draining rivers one to two orders of magnitude higher than in the interior. This is consistent with the difference in slope of the χ-plots and migration of the intervening divide.

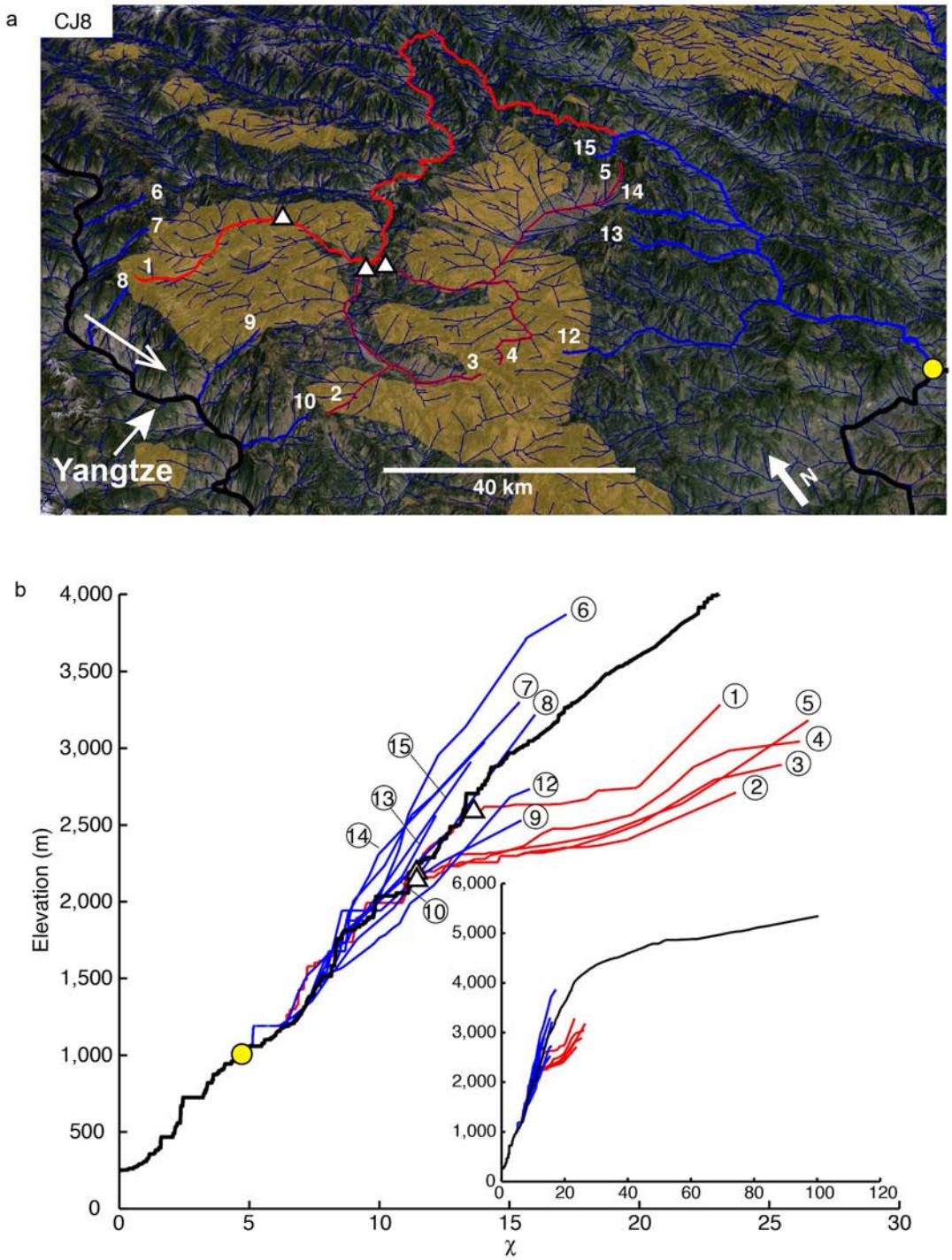

Extended Data Figure 6 | River courses and χ-plots for the region of low-relief landscape CJ8 in the Yangtze drainage. See Fig. 1 for location. Figure format as in Extended Data Fig. 3. **a**, Perspective view of the landscape. The low-relief surface is shaded and the courses of 14 rivers are keyed by colour and number to the χ-plots in **b**. **b**, Graph of χ-plots for rivers shown in **a**. Rivers 1–5 are shifted into the area-loss field, but do not show evidence of recent capture. Remaining rivers are either in equilibrium or are shifted into the area-gain field.

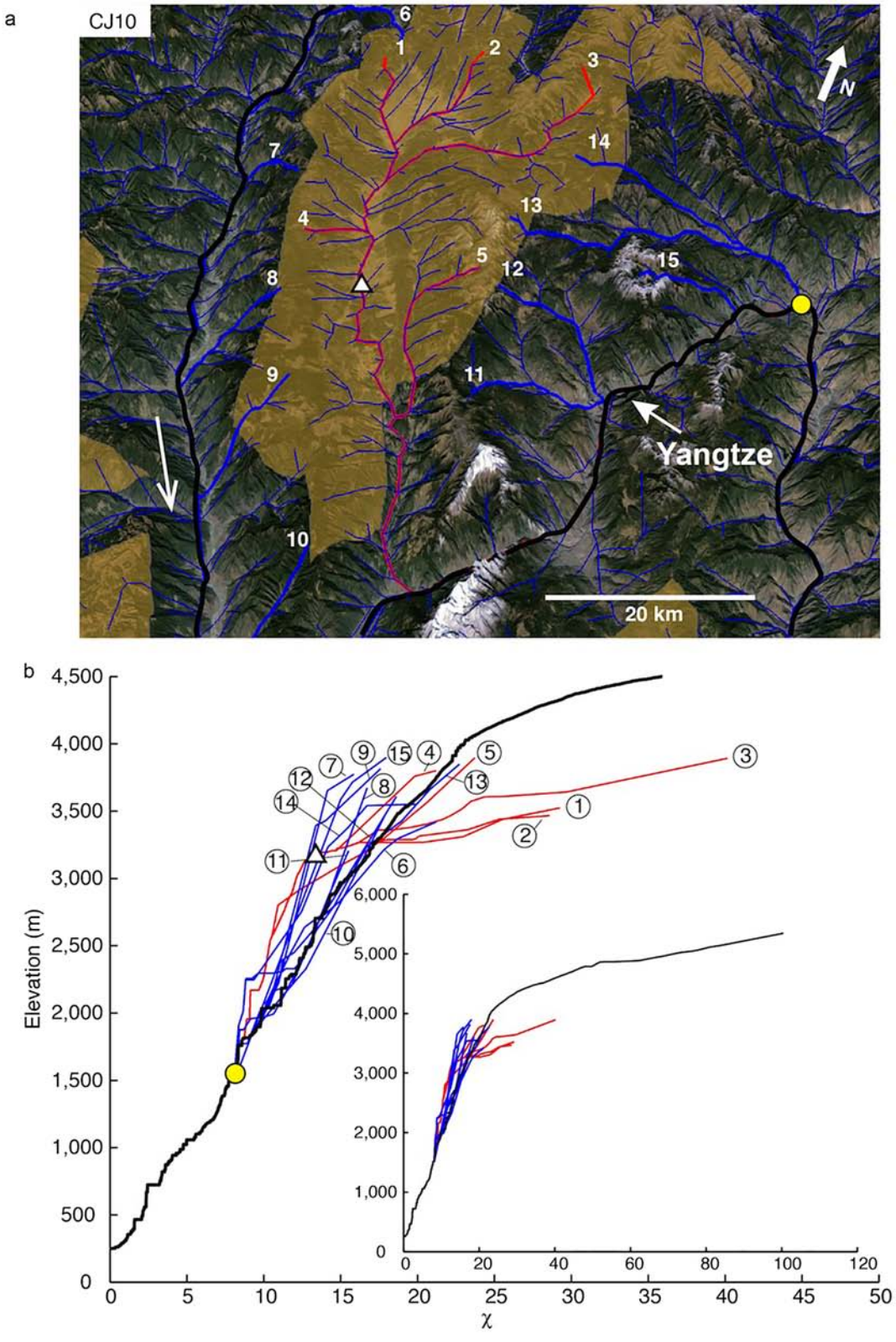

Extended Data Figure 7 | River courses and χ-plots for the region of low-relief landscape CJ10 in the Yangtze drainage. See Fig. 1 for location. Figure format as in Extended Data Fig. 3. a, Perspective view of the landscape. The low-relief surface is shaded and the courses of 15 rivers are keyed by colour and number to the χ-plots in **b**. **b**, Graph of χ-plots for rivers shown in **a**. Rivers 1–3 are shifted into the area-loss field, and may have been captured given their steep, common lower reach. This interpretation would include rivers 4 and 5. Remaining rivers are either in equilibrium or are shifted into the area-gain field.

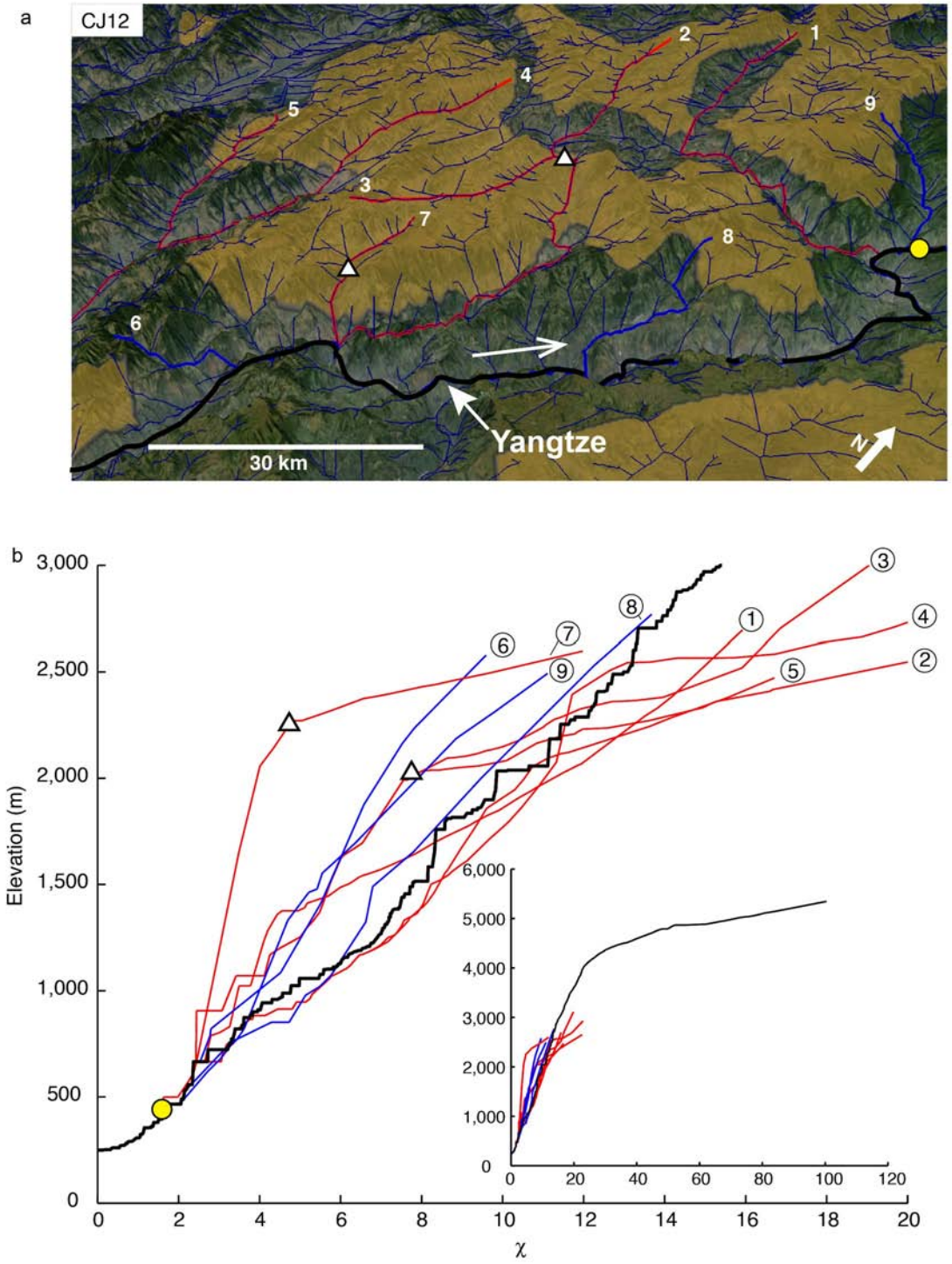

Extended Data Figure 8 | River courses and χ-plots for the region of low-relief landscape CJ12 in the Yangtze drainage. See Fig. 1 for location. Figure format as in Extended Data Fig. 3. **a**, Perspective view of the landscape. The low-relief surface is shaded and the courses of nine rivers are keyed by colour and number to the χ-plots in **b**. **b**, Graph of χ-plots for rivers shown in **a**. Rivers 1–5 are shifted into the area-loss field. Tributaries 2, 3 and 7 show evidence of recent capture. Tributaries 6, 8 and 9 are shifted into the area gain field.

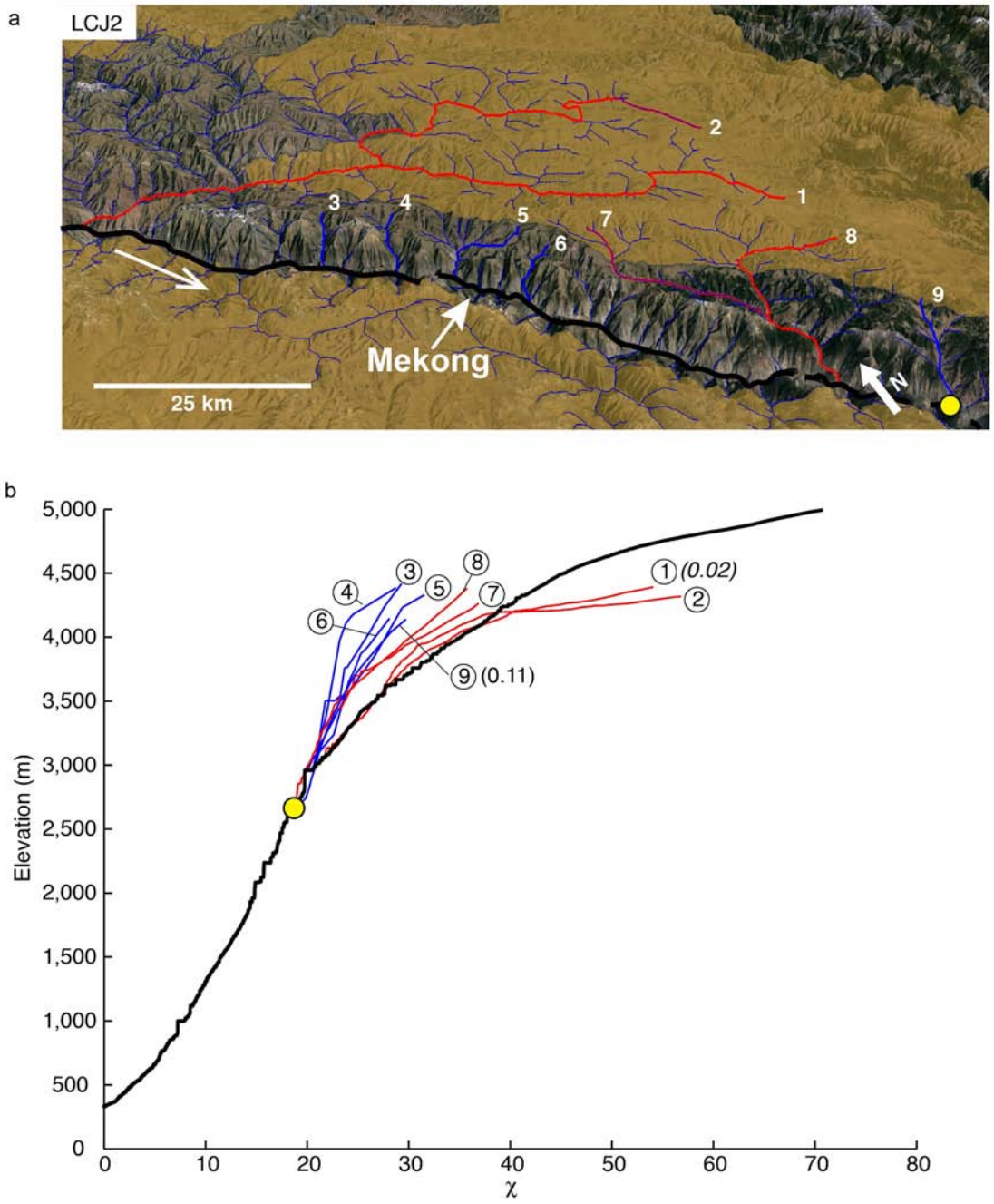

Extended Data Figure 9 | River courses and χ-plots for the region of low-relief landscape LCJ2 in the Mekong drainage. See Fig. 1 for location. Figure format as in Extended Data Fig. 3. **a**, Perspective view of the landscape. The low-relief surface is shaded and the courses of nine rivers are keyed by colour and number to the χ-plots in **b**. **b**, Graph of χ-plots for rivers shown in **a**. Rivers 1 and 2 are shifted into the area-loss field. Tributaries 7 and 8 indicate recent capture. Tributaries 3–6 are shifted into the area-gain field. Numbers in parentheses are erosion rates derived from ^{10}Be concentrations[16] or from thermochronometry (in italics)[19] and indicate rates much higher in exterior basin 9 relative to the interior.